J Electroceram (2006) 16:363–368
DOI 10.1007/s10832-006-9880-6

Cation distribution and magnetic behavior of $Mg_{1-x}Zn_xFe_2O_4$ ceramics monitored by Mössbauer spectroscopy

S. Ounnunkad · P. Winotai · S. Phanichphant

© Springer Science + Business Media, LLC 2006

Abstract The properties of magnesium ferrites, $Mg_{1-x}Zn_xFe_2O_4$ with $0.0 \leq x \leq 0.5$, were investigated by means of powder X-ray diffraction, magnetization, Mössbauer spectroscopy, and scanning electron microscopy. The ferrites were prepared by conventional solid-state reaction using a mixed oxide method. All XRD patterns revealed only the monophasic spinel characteristic structure of $MgFe_2O_4$. The lattice parameters increased with the increasing of Zn content. Saturation magnetization (M_S) of the ferrites was discussed with respect to Zn substitution. M_S values increased with Zn content up to $x = 0.35$ and then decreased thereafter. Mössbauer results showed Fe^{3+} ion distribution between tetrahedral and octahedral sites and the effect of Zn ions on ferrimagnetic order. The line-broadening of the Mössbauer spectra increased with substituting Mg with Zn ions due to disruption of the local magnetic order. The SEM micrographs of the sintered bodies showed irregular shape in the order of ∼5–6 μm.

Keywords Magnesium ferrites · Cation distribution · Saturation magnetization · Mössbauer · Magnetic

1 Introduction

Spinel ferrites have intensively studied and developed for uses as ferrimagnetic materials [1, 2], catalysts and pigments [3, 4], sensing materials [4–7], in high density memory devices, ferrofluid, drug carriers, and MRI contrast agents [8]. Magnesium ferrite ($MgFe_2O_4$) is a soft magnet (space group *Fd-3m*) with low coercivities and high resistivities. Both properties are rendered itself for industrial applications in microwave devices, satellite communication, transformers, audio-video in digital recording, and as ferrite core [9]. The formula and distribution of magnesium ferrite are represented as $(Mg^{2+}_{1-x}Fe^{3+}_x)[Mg^{2+}_xFe^{3+}_{2-x}]O^{2-}_4$, where round and square brakets denoted tetrahedral (A) and octahedral $[B]$ sites respectively and x represents the degree of inversion (defined as the fraction of the (A) sites occupied by Fe^{3+} cation) [4, 10]. In ferrite, the exchange interaction aligns the magnetic moments of the ions on (A) sites anti-parallel to those on the $[B]$ sites. The interaction is called "$Fe^{3+}(A)$-O-$Fe^{3+}[B]$ superexchange interaction" which resulting in the amount of magnetization. The magnetic properties depend on magnetic cation distribution between (A) and $[B]$ sites in $MgFe_2O_4$ [11, 12]. Flexibility of cation distribution in $MgFe_2O_4$ is monitored by various techniques such as refinement of XRD and neutron diffraction patterns, magnetization measurement and Mössbauer spectroscopy. Recently, Šepelák et al. showed that changing in the magnesium ferrite was caused by the high-energy milling process. This process led to an enhancing in the magnetization of $MgFe_2O_4$ corresponding to the mechanically induced cation distribution, redistribution and spin canting [4, 11, 12]. Lee et al. studied the effect of Cr ions on magnetic properties of $MgFe_2O_4$ [2]. It was found that with the increasing Cr content the ferrimagnetic (antiferromagnetic) order was transformed into superparamagnetic state belonging to cation distribution, magnetic dilution and disruption of the magnetic ordering. Therefore, the saturation magnetization and Curie temperature were decreased with increasing Cr doping content. The effect of Li^+ ion on crystal symmetry

S. Ounnunkad (✉) · S. Phanichphant
Nanoscience Research Laboratory, Department of Chemistry, Faculty of Science, Chiang Mai University, Chiang Mai 50200, Thailand
e-mail: sounnunkad@yahoo.com; suriyacmu@yahoo.com

P. Winotai
Department of Chemistry, Faculty of Science, Mahidol University, Rama VI Rd., Bangkok 10400, Thailand

and cation ordering of $MgFe_2O_4$ was determined by Antic's group [13]. Solid solutions of $Li_xMg_{1-2x}Fe_{2+x}O_4$ with $x \geq 0.40$ were of the ordered spinels with a primitive cubic cell and space group $P4_332$. The samples with $x \leq 0.35$ were of spinels with a face-centered cubic cell and space group *Fd-3m* [13].

In present work, the effect of Zn^{2+} non-magnetic ions on cation distribution and magnetic behavior of solid-state derived $Mg_{1-x}Zn_xFe_2O_4$ ceramics has been investigated. The study showed the enhancement of magnetization of the ceramics with respect to the cation distribution, magnetic properties and Mössbauer parameters.

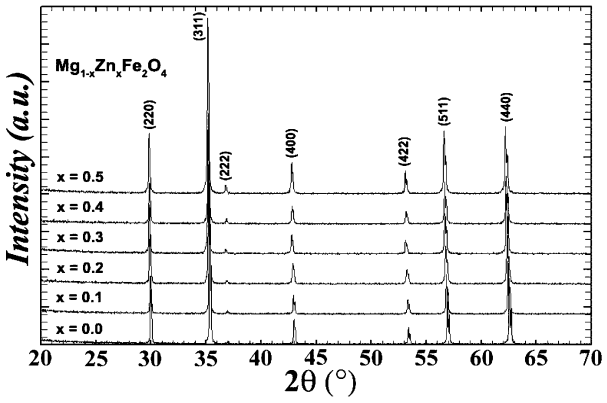

Fig. 1 XRD patterns of $Mg_{1-x}Zn_xFe_2O_4$ ceramics

2 Experimental details

Polycrystalline Zn-substituted magnesium ferrites, $Mg_{1-x}Zn_xFe_2O_4$ with $x = 0.0$–0.5, were investigated and prepared by a conventional solid-state reaction. The accurate weight of dehydrated metal oxides (99.0% Fe_2O_3, 98.0% MgO and 99.0% ZnO) were first ground and mixed homogenously in an agate mortar. Stoichiometric powdered mixtures were calcined at 1000°C for 1 h in an oxygen atmosphere. The calcined powders were reground and sieved through a 1-micron size sieve. The resultant powders were pelletized at 2000 psi with small amount of 2% wt PVA binder and then sintered at 1200°C for 24 h in an oxygen atmosphere.

The spinel phase materials were proved from powder X-ray diffraction (XRD) data by using a Bruker Axs Diffractometer with Cu Kα radiation. The diffraction patterns were refined by the Rietveld method using FULLPROF-SUITE 2000 package computer program [14]. *M-H* hysteresis loops were recorded by magnetometer (Walker Scientific) and the saturation magnetizations (M_S) were calculated from the equation of law of approach to saturation [15]. The room temperature Mössbauer spectra were recorded by a constant acceleration Mössbauer spectrometer (CMTE, Germany) using a 50 mCi ^{57}Co/Rh γ-ray source and the α-Fe foil was used for calibration of the velocity scale. The Mössbauer spectra were fitted by a PC-Mos II program (least square fitting). The grain and microstructure were examined by a scanning electron microscope (HITACHI S-2500).

3 Results and discussion

Figure 1 shows all XRD patterns of the spinel ferrite ceramics at room temperature. All spinel ferrites are without other intermediate phases such as MgO, ZnO, α-Fe_2O_3 (hematite), and γ-Fe_2O_3 (maghemite). The typical refined XRD patterns of the ceramics are shown in Fig. 2 corresponding to the spinel ferrite of the reference $MgFe_2O_4$ with cubic symmetry and space group *Fd-3m*. The lattice parameter of the spinel ferrites increased with the substitution of Mg by Zn, as shown in Fig. 3 [14]. The changing of lattice parameter was due to the relatively large radii of Zn^{2+} (0.88 Å) as compared with that of Mg^{2+} (0.86 Å) in the six-fold coordination (octahedral).

The saturation magnetizations (M_S) and coercivities (H_C) of spinel ferrite ceramics at room temperature are shown in Figs. 4 and 5 respectively. It was found that the spinel ferrites exhibited abnormal magnetic behavior which the saturation magnetization increased, reaching a maximum ($0.30 \leq x \leq 0.40$) when x was approximately 0.35 [10] and then decreased, as Zn content increased, suggesting that the existence of canted spins, redistribution of Fe^{3+} ions in both sites, changing of lattice parameter and disruption of magnetic order. The improvement of M_S was controlled by the addition of Zn ions into the $MgFe_2O_4$ ceramics. An increment in M_S at first was contributed by the spin canting and the enhancement of $Fe^{3+}(A)$-O-$Fe^{3+}[B]$ superexchange interaction with the increasing of Fe ions at (A) site observed from Mössbauer spectra. However, the decreasing in M_S after reaching to a maximum could be due to the effects of increasing in the unit cell volume and Fe^{3+} ion redistribution into (A) site when Zn was added. In general, the magnetization is a difference of magnetic moments at (A) and [B] sites. The more Fe^{3+} redistribution into (A) site could contribute the decreasing in overall magnetic moment. The expansion of the crystal structure weakened the superexchange interaction, $Fe^{3+}[B]$-O-$Fe^{3+}[B]$ double exchange interaction and super-transfer field. Therefore, both results made M_S falls after reaching a maximum, which resulting in the reduction of Curie temperature [2]. Figure 5 shows the decreasing in H_C values with the increasing of Zn content due to the larger grain sizes proved by SEM micrographs as illustrated in Fig. 7. It was evidence that the increasing in Zn ion promoted grain growth mechanism [17].

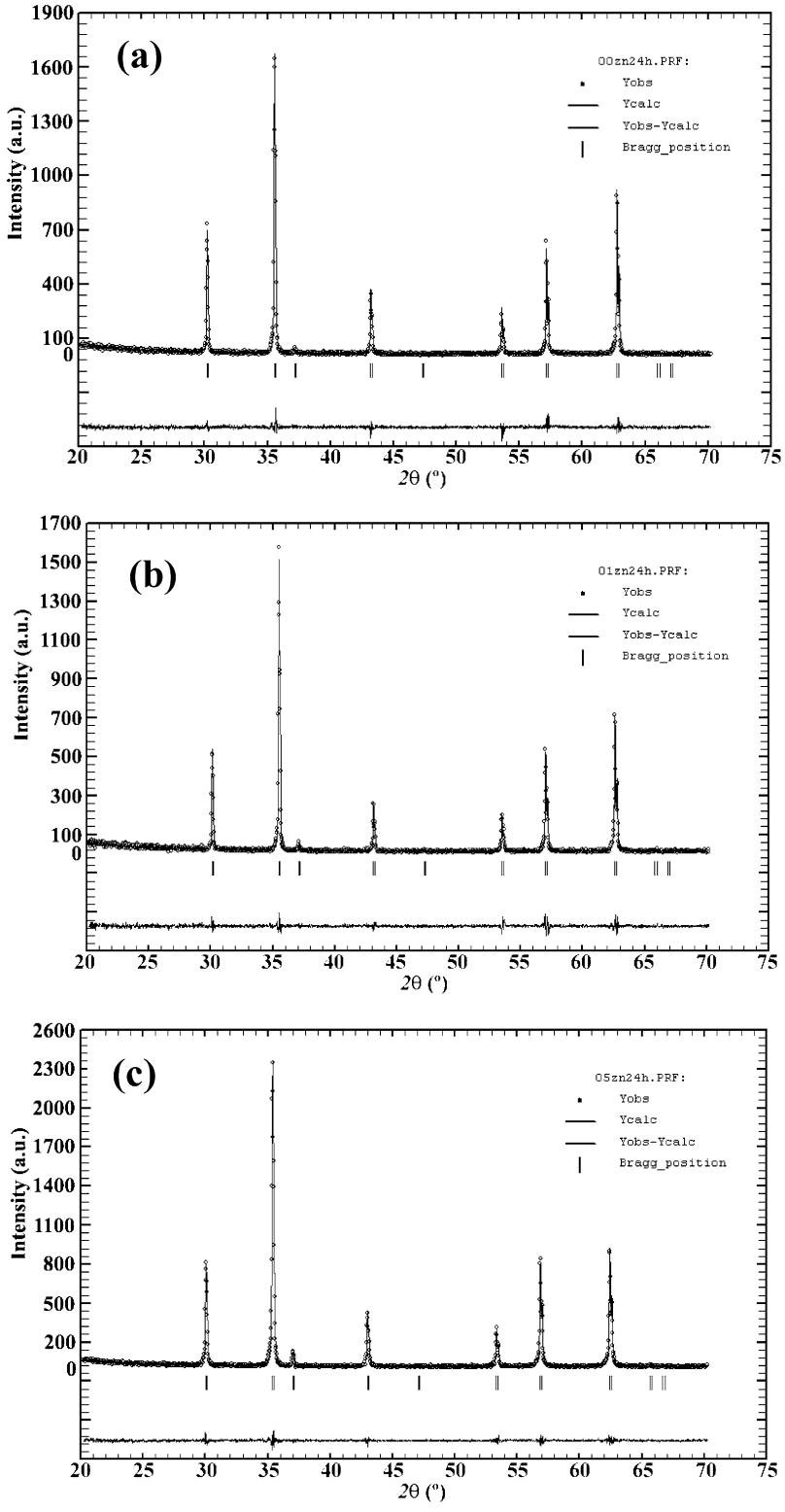

Fig. 2 Refined room temperature XRD patterns of (a) $MgFe_2O_4$, (b) $Mg_{0.9}Zn_{0.1}Fe_2O_4$ and (c) $Mg_{0.5}Zn_{0.5}Fe_2O_4$

^{57}Fe Mössbauer spectra of spinel ferrite ceramics are shown in Fig. 6. At low Zn content ($0.0 \leq x < 0.40$), the Mössbauer spectra was analyzed by using the assumption of Lorentzian line shapes and resolved into two separate six-line Zeeman splitting (two sextets) which corresponded to ^{57}Fe ions at the tetrahedral (A) and the octahedral [B] sites. The hyperfine field at (A) site was lower than that of [B] site having higher exchange interaction and internal magnetic field strength. The chemical isomer shift values of Fe ions at (A) and [B] sites were of

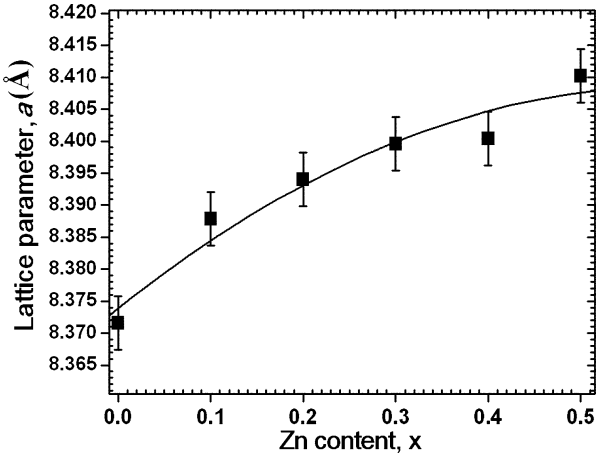

Fig. 3 Lattice parameters of $Mg_{1-x}Zn_xFe_2O_4$ ceramics

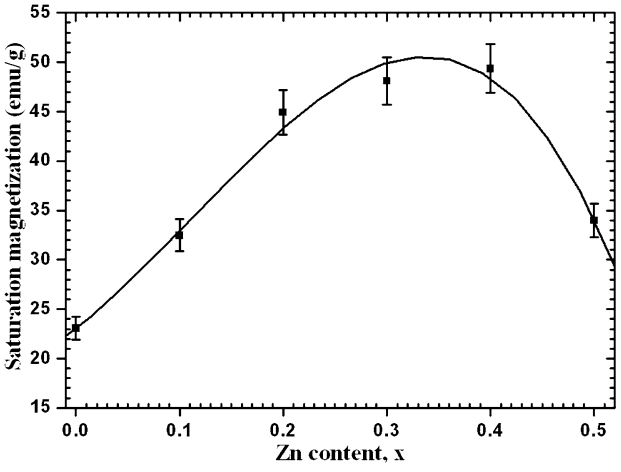

Fig. 4 Saturation magnetizations of $Mg_{1-x}Zn_xFe_2O_4$ ceramics

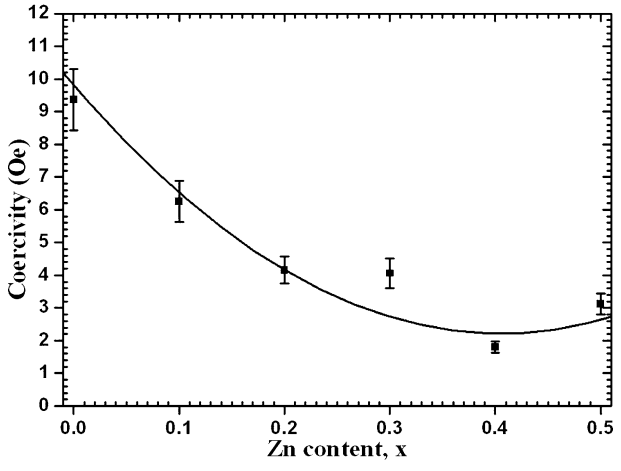

Fig. 5 Coercivities of $Mg_{1-x}Zn_xFe_2O_4$ ceramics

high-spin Fe^{3+} valence state [18]. The relative areas of the fitted Mössbauer spectra gave the Fe ion distribution for each site. As a result, the amount of Mg ions entering into $[B]$ octahedral sites could increase with increasing

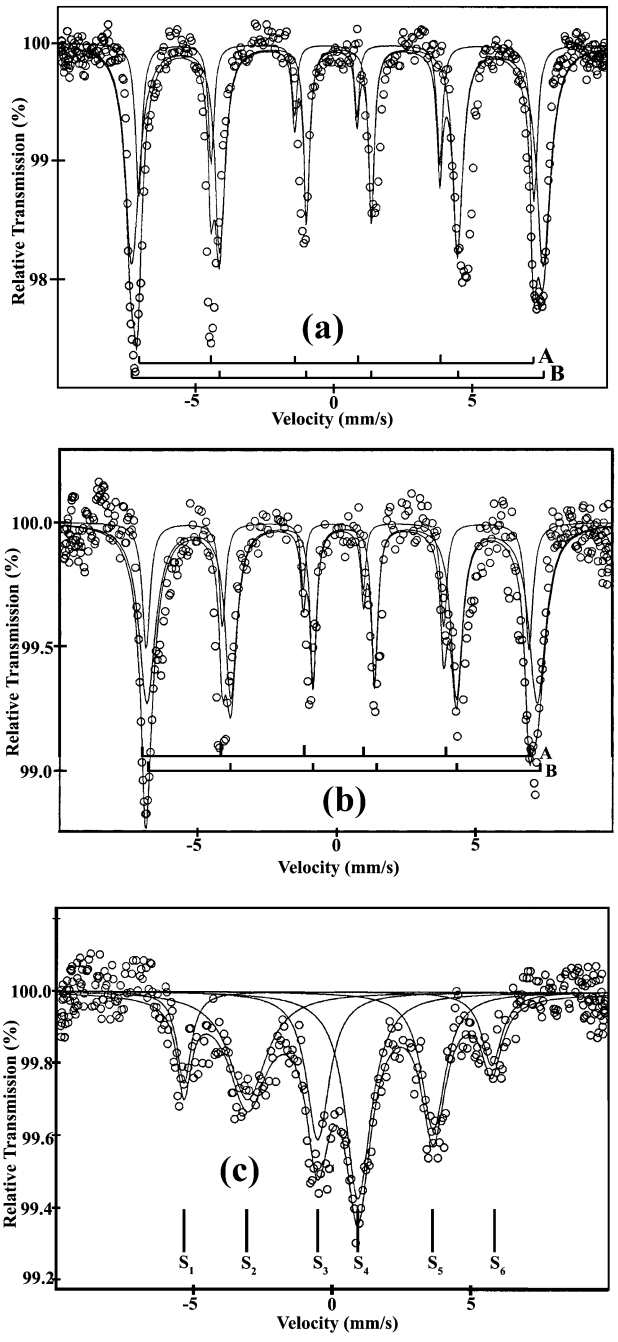

Fig. 6 Mössbauer spectra of (a) $MgFe_2O_4$, (b) $Mg_{0.8}Zn_{0.2}Fe_2O_4$ and (c) $Mg_{0.5}Zn_{0.5}Fe_2O_4$

Zn content by assuming that Zn has preference at only (A) tetrahedral sites [18]. The relative area of $[B]$ site belonging to concentration of Fe^{3+} ions on $[B]$ sites decreased due to the inversion of Fe^{3+} into (A) sites. The Fe^{3+}(A)-O-$Fe^{3+}[B]$ superexchange interaction strength was increased which resulting in higher M_S values. At high doping contents ($x \geq 0.40$) the Mössbauer spectra showed broader spectra which explained the transition peaks belonging to disruption of local

magnetic ordering and magnetic dilution with Zn ion strongly entering into (A) site (normal spinel) [9], more Fe redistribution on (A) site (increase in Mg ion occupying on [B] site) and the expansion of unit cell volume as shown in Fig. 4. It was difficult to extract the Mössbauer parameters by using the NSextet assumption. The Mössbauer data were fitted well by using NSinglet theory with six sub-components and the isomer shifts and the relative fraction parameters were obtained from this fitting process. The super-transferred magnetic fields of Fe^{3+} at the [B] sites usually increase with the number of Fe^{3+} next-nearest neighbor (A) sites [19]. Each [B] site has 6 (A) sites as the next-nearest neighbors. At the Zn doping rate, the Zn and the remaining Mg ions could occupy at (A) sites. The super-transferred fields between both sites will be reduced and the disruption of ferromagnetic order will occur. In addition, a factor attributing to reduction of super-transferred field was an effect of high expansion of unit cell volume. The Mössbauer spectra in this study demonstrated that the ferrimagnetic order was clearly disturbed and Fe^{3+}(A)-O-Fe^{3+}[B] superexchange interaction was weakened by Zn ions. These resulted in the decreasing of the M_S thereafter a maximum. All the Mössbauer parameters are listed in Table 1. Figure 7 exhibits the typical SEM micrographs of the sintered body surfaces with irregular shape in the order of ∼5–6 μm and the grain sizes could be increased with the increasing in Zn content.

Table 1 Fitted room temperature Mössbauer parameters of $Mg_{1-x}Zn_xFe_2O_4$ ceramics: the hyperfine fields (H_{hf}), the isomer shift (IS), the quadrupole splitting (QS) and the relative areas (S(%)).

x	Site	H_{hf} (kOe)	IS (mm/s)	QS(mm/s)	S(%)
0.0	A	442.8	−0.072	0.390	24.81
	B	460.5	0.199	−0.040	75.19
0.1	A	433.5	−0.070	0.372	19.91
	B	449.1	0.214	−0.080	80.09
0.2	A	427.8	−0.40	0.161	27.85
	B	435.9	0.236	−0.062	72.15
0.3	A	391.7	0.340	−0.121	47.07
	B	419.0	0.107	0.008	52.93
0.4	S_1		−6.152		13.96
	S_2		−3.545		23.09
	S_3		−0.720		15.35
	S_4		1.132		13.45
	S_5		1.183		13.50
	S_6		4.019		20.65
0.5	S_1		−5.363		6.94
	S_2		−3.073		21.51
	S_3		−0.537		17.95
	S_4		0.926		28.39
	S_5		3.641		17.45
	S_6		5.740		7.76

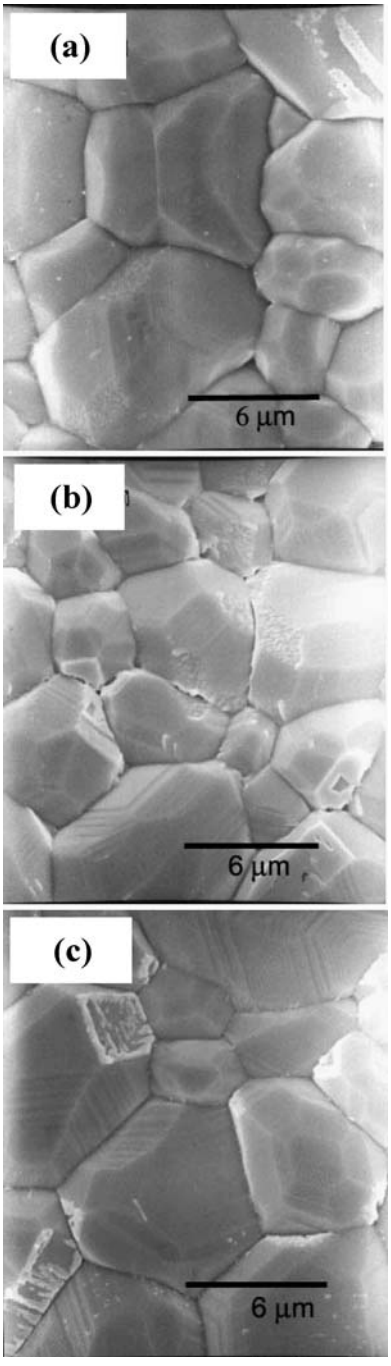

Fig. 7 SEM photographs of (a) $MgFe_2O_4$, (b) $Mg_{0.9}Zn_{0.1}Fe_2O_4$ and (c) $Mg_{0.7}Zn_{0.3}Fe_2O_4$

4 Conclusion

The optimum Zn content for enhancing magnetization of $Mg_{1-x}Zn_xFe_2O_4$ was found to be at $x = 0.35$. The M_S value was increased due to Fe^{3+} ion redistribution at both sites and the presence of the canted spins with the increasing in Zn concentration. The M_S enhancement could be caused by the increasing in superexchange interaction. After reaching the

maximum, the magnetization was dramatically decreased due to the lower superexchange interaction, unit cell expansion and the disruption of local magnetic order which observed from Mössbauer spectra data.

Acknowledgments The authors would like to thank The Development and Promotion for Science and Technology Talents Project of Thailand (DPST), the Postgraduate Education and Research Program in Chemistry (PERCH), Graduate School and Department of Chemistry, Faculty of Science, Chiang Mai University for financial supports.

References

1. G.A. Sawatzky, F. Van Der Woude, and A.H. Morrich, *Physical Review*, **187**(2), 747 (1969).
2. S.W. Lee, S.Y. An. G.Y. Ahn, and C.S. Kim, *J. Appl. Phys.,* **87**(9), 6238 (2000).
3. T. Mathew, B.S. Rao, and C.S. Gopinath, *J. Catal.*, **222**(1), 107 (2004).
4. V. Šepelák, D. Baabe, F.J. Litterst, and K.D. Becker, *J. Appl. Phys.*, **88**(10), 5884 (2000).
5. S. Tao, F. Gao, X. Liu, and O.T. Sørensen, *Mater. Sci. Eng. B*, **77**, 172 (2000).
6. N.-S. Chen, X.-J. Yang, Er.-S. Liu, and J.-L. Huang, *Sens. Actuators B*, **66**, 178 (2000).
7. N. Rezlescu, E. Rezlescu, C.-L. Sava, F. Tudorache, and P.D. Popa, *Phys. Stat. Sol. (a)*, **201**(1), 17 (2004).
8. D. Caruntu, Y. Remond, N.H. Chou, M.-J. Jun, G. Caruntu, J. He, G. Goloverda, C. ÓConnor, and V. Kolesnichenko, *Inorg. Chem.*, **41**, 6137 (2002).
9. R.A. McCurrie, *Ferromagnetic Materials: Structure and Properties* (Academic Press, London, 1994), p. 180 & 234.
10. J. Smit, *Magnetic Properties of Materials* (Mcgraw-Hill, New York, 1971), p. 21, 86 & 225.
11. V. Šepelák, D. Schultze, F. Krumeich, U. Steinike, and K.D. Becker, *Solid State Ionics*, **141–142**, 677 (2001).
12. V. Šepelák, D. Baabe, D. Mienert, F.J. Litterst, and K.D. Becker, *Scripta Mater.*, **48**, 961 (2003).
13. B.Antic, D. Rodic, A.S. Nikolic, Z. Kacarevic-Popovic, and Lj. Karanovic, *J. Alloy. Compd.*, **336**, 286 (2002).
14. www.ccp14.ac.uk
15. B.D. Cullity, *Introduction to Magnetic Materials* (Addison-Wesley, Massachusetts, 1972), vol. 347, p. 198.
16. G. Chandrasekaran and P. Nimy Sebastian, *Mater. Lett.*, **37**, 17 (1998).
17. R.V. Mangalaraja, S. Ananthakumar, P. Manohar, and F.D. Gnanam, *Mater. Lett.*, **57**, 2666 (2003).
18. S.W. Lee, S.Y. An, S.R. Yoon, I.-B. Shim, and C.S. Kim, *J. Magn. Magn. Mater.*, **254–255**, 565 (2003).
19. T.A.S. Ferreira, J.C. Waerenborgh, M.H.R.M. Mendonca, M.R. Nunes, and F.M. Costa, *Solid State Sci.*, **5**, 383 (2003).